Article

pubs.acs.org/Biomac

Self-Assembling Behavior of Cellulose Nanoparticles during Freeze-Drying: Effect of Suspension Concentration, Particle Size, Crystal Structure, and Surface Charge

Jingquan Han,[†] Chengjun Zhou,[†] Yiqiang Wu,[‡] Fangyang Liu,[§] and Qinglin Wu*[,†]

[†]School of Renewable Natural Resources, Louisiana State University AgCenter, Baton Rouge, Louisiana 70803, United States
[‡]College of Materials Science and Engineering, Central South Forestry University of Science and Technology, Changsha, China
[§]Department of Physics and Astronomy, Louisiana State University, Baton Rouge, Louisiana 70803, United States

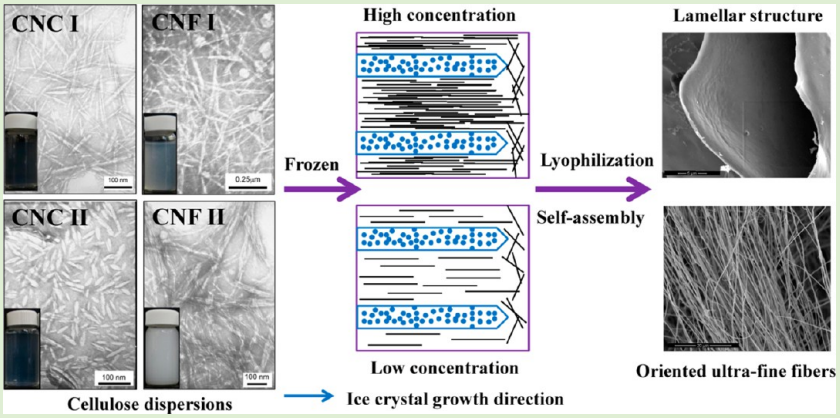

ABSTRACT: Cellulose nanocrystals and cellulose nanofibers with I and II crystalline allomorphs (designated as CNC I, CNC II, CNF I, and CNF II) were isolated from bleached wood fibers by alkaline pretreatment and acid hydrolysis. The effects of concentration, particle size, surface charge, and crystal structure on the lyophilization-induced self-assembly of cellulose particles in aqueous suspensions were studied. Within the concentration range of 0.5 to 1.0 wt %, cellulose particles self-organized into lamellar structured foam composed of aligned membrane layers with widths between 0.5 and 3 μm. At 0.05 wt %, CNC I, CNF I, CNC II, and CNF II self-assembled into oriented ultrafine fibers with mean diameters of 0.57, 1.02, 1.50, and 1.00 μm, respectively. The size of self-assembled fibers became larger when more hydroxyl groups and fewer sulfates (weaker electrostatic repulsion) were on cellulose surfaces. Possible formation mechanism was inferred from ice growth and interaction between cellulose nanoparticles in liquid-crystalline suspensions.

INTRODUCTION

Foam biomaterials with well-defined structures are desirable for a wide range of applications, including drug delivery, tissue engineering, green packaging, and automotive components.[1] They have high strength-to-weight ratios and porosities to carry and store other materials to form composites. By controlling their microstructures, the properties of the materials can be readily tuned. Among the available techniques, freeze-drying has been shown as a novel, low-cost, simple and versatile route for the preparation of foam biomaterials with controlled structures.[2] During the freezing process of an aqueous suspension, suspended particles are organized in the intervening space between growing ice crystal fronts, leading to an ordered structure after sublimation of ice crystal templates.

Cellulose nanocrystals (CNCs) and cellulose nanofibers (CNFs) have recently received a considerable amount of attention due to their intrinsically appealing properties.[3] The rod-like CNCs and needle-like CNFs are mainly prepared by controlled acid hydrolysis of native cellulose sources. For wood, mean width and length of CNCs are 5−10 nm and 100−300 nm, respectively, and the CNFs are 5−50 nm in width and several micrometers in length.[4,5] To expand their applications, much work has concentrated on the drying process of CNC and CNF aqueous suspensions.[6]

Recently, research has been attempted to use the freeze-drying technique to fabricate biomimetic cellulose foam with different microstructures and properties.[7] Lee and Deng[1] prepared cellulose microfibril foams with a lamellar channel or a cross-linked network structure using a directional freezing technique. They investigated the effect of freezing temperature and suspension concentrations on the microstructure and mechanical properties of cellulose microfibril foams. Subsequently, Dash et al.[2] fabricated cellulose nanowhisker foams with a uniform layer structure, and they discussed the

Received: February 2, 2013
Revised: March 28, 2013
Published: April 1, 2013

relationship between the freezing conditions and the microstructures obtained. However, some fundamental research still needs to be conducted in order to understand the self-organization of cellulose particles during the freeze-drying process. The lyophilization process consists of two important steps, that is, growing of the ice crystals (freezing) and sublimation of the ice molecules (drying). Upon freezing cellulose aqueous suspensions, water is frozen into ice crystals and then most cellulose particles above the critical particle size are trapped by the moving water−ice front and confined into the interstitial spaces between ice crystals. The final structure of cellulose foam is formed as ice crystals are sublimated during the drying step.[7,8] Therefore, in addition to the freezing conditions, the particle size, surface charge, suspension concentration, and their relationship with the self-assembly behavior of cellulose particles are theoretically related to the morphology and properties of the final foam. Lee and Deng[1] reported the effects of high concentrations (above 1.0 wt %) on the microstructure and mechanical properties of cellulose microfibril foams. However, little is known about the self-assembling behavior of cellulose particles during the freeze-drying process at low suspension concentrations (e.g., below 1.0 wt %).

In the present study, size-controllable cellulose particles with cellulose I and II structures were extracted from bleached wood pulp (BWP) using alkali treatment and acid hydrolysis in combination with homogenization process. The crystal structure, crystallinity, hydrogen bonding patterns, surface charge, and morphology of cellulose particles produced using different methods were compared. The dispersion state, liquid-crystalline properties and optical transmittance of cellulose aqueous suspensions were also studied. The objectives of the work were to investigate the effects of suspension concentrations (0.05 to 1.0 wt %), particle size, crystal structure, and surface charge on the self-assembling behavior of cellulose particles during the freeze-drying process. This research described the liquid-crystalline properties, supramolecular structure development, and self-assembling mechanism of cellulose particles during lyophilization, providing a fundamental guidance for the applications of cellulose nanoparticles as templates for layered scaffolds, filters, and storage materials.[2,8]

EXPERIMENTAL SECTION

Materials. Bleached wood pulp, W-50 grade of KC Flock, provided by Nippon Paper Chemicals Co., Ltd. (Tokyo, Japan), was dried overnight in a vacuum oven at 60 °C before use. Sulfuric acid (95 to 98 wt %, VMR, West Chester, PA, U.S.A.) was of analytical grade and was diluted to a concentration of 64 and 48 wt % before use. Sodium hydroxide (NaOH over 97.0% purity, ACS, MS, U.S.A.) was dissolved in distilled water to prepare a 20 wt % aqueous solution. All reagents and solvents used were of analytical grade.

Preparation of CNCs and CNFs with Cellulose I and II Structures. Approximately 30 g of BWP were pretreated by an excess of 20 wt % aqueous NaOH solution for 4 h at room temperature. The obtained slurry was filtered and thoroughly washed with distilled water until a neutral pH was reached. The pretreated wood fibers (designated as mercerized wood pulp) were then dried at 40 °C in a vacuum oven for 48 h prior to further processing. For the CNCs with cellulose I structure (designated as CNC I), dry BWP was hydrolyzed using 64 wt % sulfuric acid at a fiber-to-acid ratio of 1:20. The mixture was stirred vigorously at 45 °C for 1 h and the acid hydrolysis was immediately quenched by diluting 15-fold with cold water. The diluted solution was filtered through a piece of filter paper (Grade-5, Whatman) under vacuum. The obtained wet cream-like, off-white slurry material was then redispersed in distilled water and the mixture was stirred for 20 min. To further remove the residual acid, they were centrifuged at 26 °C for 20 min with a constant speed of 12000 rpm (Sorvall RC-5B Refrigerated Superspeed Centrifuge, Du Pont Instrument, NH, U.S.A.). The CNCs were separated from the suspension by centrifuging after each washing. After three centrifugation cycles, the ivory-colored CNC precipitate obtained was placed in regenerated cellulose dialysis tubes with a molecular weight cutoff of 12000−14000 (Fisher Scientific, Pittsburgh, PA, U.S.A.) and dialyzed against distilled water for several days until neutral pH was reached. The resultant concentration of CNC suspension was about 0.85 wt %. For the preparation of CNFs with cellulose I structure (designated as CNF I), 48 wt % sulfuric acid was used and the other conditions were identical with those for CNC I. For the preparation of CNCs and CNFs with cellulose II structure (designated as CNC II and CNF II), 64 and 48 wt % sulfuric acid were used to hydrolyze the mercerized wood pulp, respectively. All other processing conditions were the same as those used for cellulose I material.

High-Pressure Homogenization (HPH) Process. To further enhance the dispersity of obtained cellulose nanoparticles in water, mechanical homogenization was applied to the obtained aqueous suspensions. They were processed through a high-pressure homogenizer (Microfluidizer M-110P, Microfluidics Corp., Newton, MA, U.S.A.) equipped with a pair of Z-shaped interaction chambers (one 200 μm ceramic, and one 87 μm diamond) under an operating pressure of 207 MPa. The CNC and CNF suspensions passed through the interaction chamber at a rate of 135 mL/min for five passes. The final fifth pass CNC and CNF suspensions without visible aggregation presented a pale bluish-purple color, indicating an excellent dispersity of CNCs and CNFs in aqueous suspensions. The concentration of homogenized CNC and CNF suspensions was 0.7 wt %. The concentration of each homogenized suspension was adjusted to the target levels by adding or evaporating water from the original suspensions. For the preparation of suspensions with higher concentrations, suspensions at lower concentrations were evaporated under vacuum at 65 °C with a rotational speed of 30 rpm in a rotary evaporator (RE300, Yamato Scientific America Inc., Santa Clara, CA, U.S.A.). The processing time was about 20−40 min, depending on the initial and desired concentrations. The concentration of each suspension was determined gravimetrically through weighing 3 g of each suspension before and after the evaporation of water in air (heating for 25 min in an oven at 100 °C). The final CNC and CNF suspensions were sealed in glass containers and stored at 5 °C in a refrigerator. The total yield of homogenized CNCs and CNFs (both I and II) was approximately 35% (based on the initial BWP weight), which was close to the values reported in the literature.[5,9]

Lyophilization. The obtained CNC (I, II) aqueous suspensions and CNF (I, II) colloidal suspensions were freeze-dried at four dilute concentration levels (i.e., 0.05, 0.1, 0.5, and 1.0 wt %) to investigate the detailed morphology development and self-assembling mechanism of CNCs and CNFs during lyophilization. The corresponding volume concentrations were, respectively, 0.03, 0.07, 0.34, and 0.67 vol% based on a cellulose density of 1.5 g/cm.[3,10] Approximately 200 mL of each suspension at a certain concentration level was poured into a 300 mL fast-freeze-drying flask (FreeZone, Labconco Corp., Kansas, MO, U.S.A.) and then was quickly frozen in an ultra-low-temperature freezer at −75 °C for about 2 h. After being completely frozen, the samples were immediately transferred to a freeze-dryer (FreeZone plus 2.5 L, Labconco Corp., Kansas, MO, U.S.A.) and freeze-dried at a sublimating temperature of −88 °C under vacuum for three days to sublimate the solvent water directly from solid phase to gas phase. The final freeze-dried samples were sealed in plastic bags before performing further characterizations.

Fourier Transform Infrared Spectrometry (FTIR). FTIR spectra of raw BWP, CNC I, CNF I, CNC II, and CNF II were measured using a Bruker FTIR analyzer (Tensor-27, Bruker Optics Inc., Billerica, MA). All spectrum were obtained in a transmittance mode on a Zn/Se ATR crystal cell at room temperature. For each measurement, approximately 5 mg of the freeze-dried powder samples were pressed into the sample chamber of the FTIR equipment, and 64 scans were

taken with a resolution of 4 cm^{-1} and a spectral range of 4000−600 cm^{-1}. Three replicated measurements were recorded for each condition.

Wide-Angle X-ray Diffraction (WXRD). WXRD patterns of the untreated BWP, CNC I, CNF I, CNC II, and CNF II were measured using a Bruker/Siemens D5000X-ray automated powder X-ray diffractometer. Before testing, each freeze-dried sample was dried again in a vacuum oven at 60 °C for 24 h to remove moisture. The WXRD data were generated by a diffractometer with Cu Kα radiation (λ = 1.542 Å) at 40 kV and 30 mA over the angular range 2θ = 5−40°, a step size of 0.02°, and a step time of 2.0 s (1.0 h per scan). The data were further analyzed using the MDI Jade 6.5.26 software (Serial No.: MDI-R99691, Materials Data Inc., Livermore, California). For each sample, the background was fitted with a software-generated cubic-spline function. Subsequently, the whole pattern was smoothed by a parabolic filter to reduce excess noise.

The degree of crystallinity or crystallinity index (CI, %) for each sample was determined using eq 1[11]

$$\mathrm{CI}(\%) = 100\frac{I_{\max} - I_{\mathrm{am}}}{I_{\max}} \quad (1)$$

where $I_{\max}$ is the maximum intensity of the principal peak and I_{am} is the intensity of diffraction attributed to amorphous cellulose. The CI values were calculated based on the original data without fitting background.

Transmission Electron Microscopy (TEM). For the TEM analysis, concentrations of the aqueous suspensions were diluted to 0.05−0.1 wt %. The diluted suspensions were treated with an ultrasonic bath (Model 3510, Branson, MS) prior to the TEM operation. A droplet (5 μL) of diluted suspension was negatively stained with a droplet (5 μL) of 2 wt % uranyl acetate for about 2 min to enhance the contrast of TEM images. Then the mixture was immediately deposited on the surface of a 400-mesh carbon-coated copper grid. The excess liquid on the grid was absorbed by using a tiny piece of filter paper to touch the edge of the grid. The morphology of obtained CNCs and CNFs (I and II) was characterized by using Transmission Electron Microscope (JEOL 100CX, JEOL, Inc., Peabody, MA) with an accelerating voltage of 80 kV. The particle dimension was calculated with TEM images using ImageJ 1.45k software (Rasband, W.S., ImageJ, U.S. National Institutes of Health, Bethesda, MD, http://imagej.nih.gov/ij/, 1997−2011). For each sample, 100 particles were randomly selected and measured from several TEM images. The width was defined as the largest dimension measured along each particle, perpendicular to its long axis.[12] Statistical parameters of particle size were calculated using the Origin 8.5.0 software (SR1 b161, OriginLab Corp., Northampton, MA).

Polarized Optical Microscopy (POM) Observations. The 1.0 wt % sample suspensions were transferred into a paired slide glass cell with a 0.5 mm thick spacer and observed using an Olympus BH-2 polarization optical microscope (Olympus Optical Co., LTD, Tokyo, Japan) equipped with a 530-nm retardation plate at room temperature. Each sample was allowed to stand overnight at 30 °C to achieve the slow evaporation of water on the sample edge. The texture of the liquid crystal phase was examined between a pair of crossed polarizers and the pictures were taken with a digital camera.

Optical Transmittance. The CNC and CNF (I and II) aqueous suspensions with concentrations of 0.05−1.0 wt % were introduced into a UV quartz cuvette with PTFE cover (dimension of 45 × 12.5 × 12.5 mm, and layer thickness of 10 mm). The optical transmittance of each aqueous suspension was measured at wavelength from 300 to 800 nm using a UV−vis spectrophotometer (Evolution 600 PC, Thermo Electron Corp., U.S.A.). The data was collected at a scan speed of 240 nm/min and a bandwidth of 2 nm. The transmission spectra were measured using distilled water as a reference to correct the transmittance of the dispersions. All tests were carried out at room temperature. The mean transmittance of each sample was calculated by averaging the transmittances over the wavelength ranging from 300 to 800 nm.

Field Emission Scanning Electron Microscopy (FE-SEM). Prior to the FE-SEM observation, all freeze-dried samples were vacuum-dried at 40 °C for 48 h. The morphology of the freeze-dried samples was examined by a FE-SEM (FEI QuantaTM 3D FEG Dual Beam SEM/FIB, Hillsboro, Oregon, U.S.A.) at an accelerating voltage of 5.0 kV. Before images were acquired, samples were mounted on SEM aluminum stubs with conductive carbon tape and sputter-coated with gold under vacuum at 20 mA for 2 min. The particle dimension was obtained from the analysis of FE-SEM images using ImageJ 1.45k software (Rasband, W.S., ImageJ, U.S. National Institutes of Health, Bethesda, MD, http://imagej.nih.gov/ij/, 1997−2011). For each sample, 100 particles were randomly selected and measured from several FE-SEM images. The statistical analysis was performed using Origin 8.5.0 software (SR1 b161, OriginLab Corp., Northampton, MA).

Surface Charge Measurements. The zeta potential values (ζ, mV) of CNC I, CNC II, CNF I, and CNF II in aqueous suspensions were determined by a ZetaTrac analyzer (MicroTrac Inc., Largo, FL, U.S.A.) based on the principles of dynamic light scatting. A 3 mW laser source with a 780 nm wavelength was used as light source. Each sample suspension (0.05 wt %) was measured three times at 25 °C and pH of 7.0. The particular concentration of 0.05 wt % was within the proper range where the electric double layers on the cellulose particles barely overlap with each other.[13] To further determine the surface charge of dried samples, X-ray photoelectron spectroscopy (XPS) was performed on the freeze-dried samples using a Specs PHOIBOS-100 spectrometer (SPECS, Berlin, Germany) with a Al Kα irradiation (1486.61 eV) at 10 kV and 10 mA. Each sample was mounted onto a holder with a piece of double-sided conductive tape and then placed in a vacuum in the range of 1 to 5 × 10^{-9} Torr. Samples were analyzed at a takeoff angle of 85° with respect to their surfaces. Survey scans were recorded with 1.0 eV step and 40 eV analyzer pass energy, while high-resolution spectrum of Na 1s and S 2p were recorded with 0.1 eV step and 40 eV analyzer pass energy. The Specslab 2.25 software was used to subtract the noise from XPS spectra to smooth the data. No degradation of the specimens during the XPS analyses was detected. The atomic ratio of sulfur to oxygen (S/O) was calculated from corresponding peak area based on the following equation:

$$\mathrm{S/O} = (A_{\mathrm{O}}/A_{\mathrm{C}}) \times (S_{\mathrm{S}}/S_{\mathrm{O}}) \quad (2)$$

where A_{O} and A_{C} are the integrated peak areas for oxygen and sulfur, respectively. S_{S} (0.54) and S_{O} (0.66) are the corrected sensitivity factors.

RESULTS AND DISCUSSION

Cellulose Structure and Hydrogen Bonding by FTIR. The FTIR spectra of BWP, CNC I, CNF I, CNC II, and CNF II are shown in Figure 1. The broad band of stretching vibrations of CH and OH groups within 3650−3000 cm^{-1} region was observed in all spectra, showing the principal functional groups found in lignocellulosic materials.[14,15] The

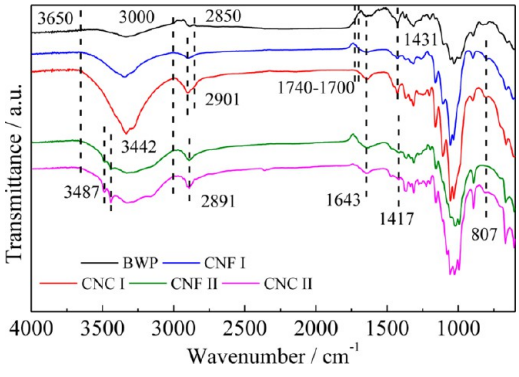

Figure 1. FTIR spectra of BWP, CNC I, CNF II, CNC II, and CNF II.

dx.doi.org/10.1021/bm4001734 | Biomacromolecules 2013, 14, 1529−1540

intense peak around 1643 cm^{-1} in all spectrum corresponds to the O−H bending of adsorbed water.[16] Although the FTIR samples were dried, the water adsorbed in the cellulose molecules was difficult to be removed completely due to the cellulose−water interaction.[17]

The absorbance band within 1740−1700 cm^{-1} is attributed to the C═O stretching of methyl ester and carboxylate groups in pectin, the acetyl and uronic ester groups of the hemicelluloses or to the ester linkage of carboxylic group of the ferulic and *p*-coumaric acids of lignin and hemicelluloses.[18,19] In addition, lignin presented the characteristic peak at 2850 cm^{-1} originating from C−H stretching vibration, the peak at 830 cm^{-1} attributed to an aromatic C−H out-of-plane vibration and absorbance band in the range 1500−1600 cm^{-1} corresponding to the aromatic skeletal vibration.[15,18] However, for the BWP, the absence of these signals in the spectra clearly verified the complete absence of lignin, pectin, and hemicellulose. Therefore, the BWP used in this study was confirmed to contain only cellulose. After sulfuric acid hydrolysis, no significant differences were observed in the spectrum of CNC I and CNF I compared with that of BWP, indicating that the cellulose molecular structure was not changed in the case of acid hydrolysis.[16,20]

After BWP was subjected to the 20 wt % NaOH treatment, the spectra of CNC II and CNF II were different from those of BWP, CNC I, and CNF I. As shown in Figure 1, compared with CNC I and CNF I, the spectra of CNC II and CNF II presented the two small bands at 3487 and 3442 cm^{-1} that were assigned to the intramolecular hydrogen bonding in cellulose II.[21] The maximum absorbance of CH stretching vibrations in methyl and methylene was also shifted from 2901 to 2890 cm^{-1}, influenced by the transformation related to the change of intra- and intermolecular bonds.[22] The absorbance peaks at 2894 cm^{-1} became sharper for CNC II and CNF II, showing a cellulose II crystal structure.[23] The band at 1431 cm^{-1} assigned as symmetric CH_2 bending was weakened and shifted to a lower wavenumber 1419 cm^{-1}, indicating development of new inter- and intramolecular hydrogen bonds and a change of the conformation of CH_2OH at C-6 from the *tg* to the *gt* form.[22] The bands at 1319 cm^{-1} assigned as CH_2 wagging, 1203 cm^{-1} attributed to C−OH in-plane at C-6 bending, 1161 cm^{-1} corresponding to C−O−C asymmetric stretching at β-glucosidic linkage, 1031 cm^{-1} ascribed to C−O at C-6 stretching, 983 cm^{-1} arisen from C−O stretching at C_6, and 897 cm^{-1} assigned as C−O−C asymmetric stretching were shifted to 1313, 1197, 1157, 1022, 993, and 894 cm^{-1}, respectively, indicating the transition from cellulose I to II.[22,23] In addition, the appearance of the peak at 1227 cm^{-1} assigned as C−OH bending in plane at C_6, the disappearance of the band at 1105 assigned as ring stretching in plane, the increasing intensity of the band near 894 cm^{-1} assigned as C−O−C asymmetric stretching at the β-(1−4)-glycosidic linkage and 668 cm^{-1} assigned as COH out-of-plane bending were also representative indexes of the conversion into cellulose II.[22−24]

Cellulose particles prepared with sulfuric acid had negatively charged surfaces due to the esterification of hydroxyl groups by sulfate ions. CNC I and CNF I both present the symmetrical C−O−S vibration at 807 cm^{-1} associated with the C−O−SO_3 group.[25] However, the sulfate content of CNC II and CNF II was too low to be detected by FTIR. It was thus inferred that CNC I and CNF I carried more sulfate groups on their surfaces, which was further determined by zeta potential (Table 1) and XPS experiments (Figure 6d).

Table 1. Dimension Parameters and Zeta Potential of Raw Wood fiBer, CNC, and CNF (I and II)

sample	dimension	mean ± std dev[a] (nm)	aspect ratio[b]	zeta potential (mV)
wood fiber	length	>300000	>20.0	ND[c]
	width	15000 ± 4000		
CNC I	length	149 ± 40	16.6	−57.07 ± 1.06
	width	9 ± 2		
CNF I	length	732 ± 208	36.6	−32.61 ± 1.12
	width	21 ± 7		
CNC II	length	46 ± 18	9.4	−0.63 ± 0.08
	width	5 ± 1		
CNF II	length	616 ± 200	38.0	ND
	width	16 ± 4		

[a]Based on 100 samples per group. [b]A ratio of mean sample length to mean sample width. [c]Not determined.

The hydrogen bonding patterns of cellulose I and II are known to be different. Therefore, the number of hydrogen bonding sites changes during the transition of crystal structure. The IR index (i.e., a ratio of IR intensity at a given wavenumber to that at the reference wavenumber) values based on the absorbance peaks at 894 cm^{-1} was used to analyze the conformation and hydroxyl intensity changes from cellulose I to II during alkaline treatment.[26] It was calculated that the OH stretching vibration within the region 3100 to 3800 cm^{-1} of cellulose II was higher than that of cellulose I. For example, the IR index values for CNC I and CNC II at 3338 cm^{-1} are 0.851 and 1.030, respectively. The increased IR index values indicated that the resulting CNC II had more −OH groups on the crystal surface, which promoted the occurrence of hydrogen bonding.

Cellulose Structure and Crystallinity Index by WXRD. The X-ray diffractograms of BWP, CNC I, and CNC II are shown in Figure 2a. The WXRD spectra of BWP and CNC I were nearly identical, indicating that the crystalline structure of native cellulose was maintained during the acid hydrolysis. Both X-ray diffraction diagrams of BWP and CNC I exhibited a sharp high peak at 2θ = 22.6° and two overlapped weaker diffraction peaks at 2θ = 15.1 and 16.6°, assigned to (002), (101), and ($10\bar{1}$) planes, respectively, indicating the crystallographic form of cellulose I.[27] Compared with BWP, the peak for the (101) plane (2θ = 15.1°) became more intense and separated from the ($10\bar{1}$) (2θ = 16.6°) peak for CNC I, as reported previously.[28]

Upon the pretreatment of BWP in the 20 wt % NaOH solution, the peaks at 2θ = 15.1° and 2θ = 16.6° disappeared and a new peak at 2θ = 12.2° ($1\bar{1}0$) formed. The (200) peak at 2θ = 22.6° was split into two weaker peaks located at 2θ = 20.0° (110) and 2θ = 21.9° (200) with similar intensities, suggesting the transformation of crystalline structure from cellulose I to cellulose II.[15,29] The rearrangement in intermolecular hydrogen bond and agglomeration between the chains during mercerization process led to the polymorphic transformation from "parallel" chains in cellulose I to "antiparallel" chains in cellulose II.[26]

The X-ray diffraction patterns of CNF I and CNF II are shown in Figure 2b. Three cellulose I peaks at 2θ = 15.1° (101), 16.6° ($10\bar{1}$), and 22.6° (002) were present in CNF I. After the mercerization, the pattern of CNF II exhibited the peaks located at 2θ = 12.4° ($1\bar{1}0$), 20.1° (110), and 22.1° (200), respectively, indicating the conversion of cellulose I into

dx.doi.org/10.1021/bm4001734 | Biomacromolecules 2013, 14, 1529−1540

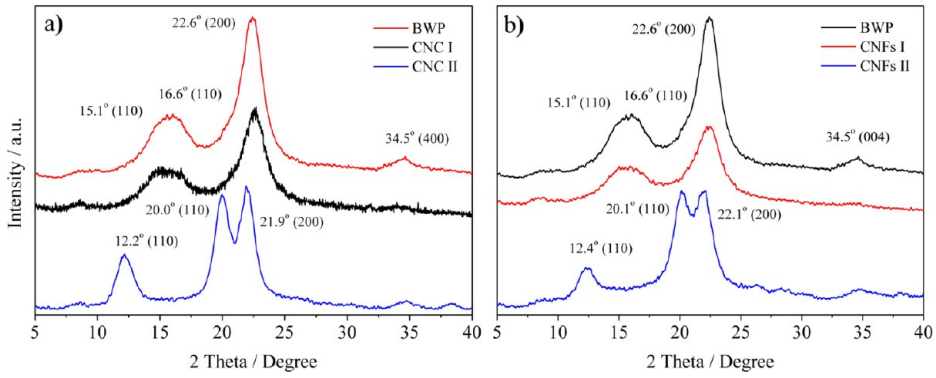

Figure 2. X-ray diffraction patterns of BWP, CNC I, and CNC II (a); CNF I and CNF II (b).

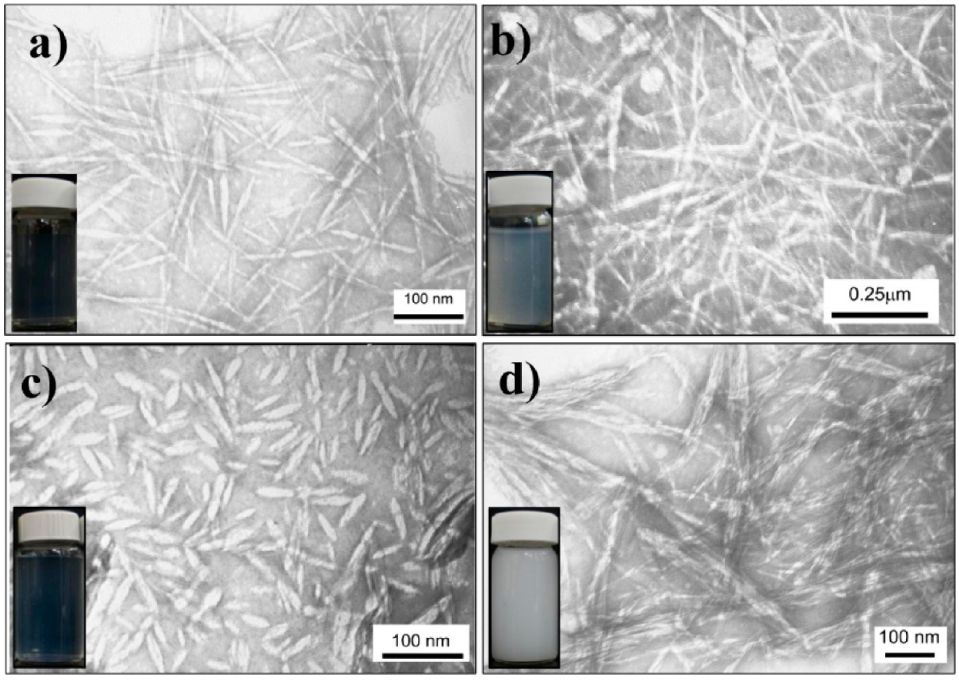

Figure 3. TEM images of CNC I (a), CNF I (b), CNC II (c), and CNF II (d) and the inset in each image representing the corresponding dispersion state of each cellulose suspension at the concentration of 1.0 wt % (all the dispersions were prepared by a 2 h stirring after preparation, and the photograph was taken after a rest of 48 h).

a weaker cellulose II crystal structure. The mercerization of cellulose fibers has three distinct steps: fiber swelling, disruption of the crystalline areas and formation of new crystalline lattice after rinsing away alkali solution. When the concentration of NaOH solution reaches to the critical value (e.g., 20 wt %, in this case), the dehydrated hydroxide ions could easily penetrate and disrupt the cellulose lattice, and the crystalline structure of the cellulose started to be swelled and relaxed. After a complete swollen state formed, the hydrated hydroxide ions penetrated the inside of the crystal and underwent a thorough reaction with the cellulose molecules.[27] The CI of untreated BWP was found to be 70.5%, which was close to the CI of microcrystalline cellulose.[30] After acid hydrolysis treatment, CNC I and CNF I exhibited decreased CI values of 66.4 and 57.6%, respectively. After the alkaline treatment and acid hydrolysis, the CI values of CNC II and CNF II were 73.6 and 71.5%, respectively. The CI values for cellulose I and II cannot be directly compared, but in general, comparable crystallinities of I and II should lead to substantially lower CI values for cellulose I.[31] The subtle differences between BWP and CNC II (or CNF II) were not significant enough to be considered as an increase in crystallinity.

Morphology of CNCs and CNFs (I and II). A comparison of the morphology of CNCs (I, II) and CNFs (I, II) isolated from BWP by different chemical treatments is presented in Figure 3. The inset images show the dispersion states of these four samples at the 1.0 wt % concentration level. Raw BWP contained large sized fiber bundles composed of many microfibrils. These fiber clusters had an average length larger than 300 μm and an average width of 15 μm (Table 1). Because of their large dimension, the BWP without any treatment did not suspend, but highly precipitated in water. After treatment with 64 wt % H_2SO_4 followed by a further HPH process, CNC I suspension was converted into the light purple transparent homogenized CNC I suspension without any visible flocculate (inset in Figures 3a and 4f). The amorphous regions of cellulose were preferentially hydrolyzed by sulfuric acid, while the crystalline regions that had a higher resistance to acid attack remained intact,[3] resulting in the isolation of nanosized cellulose crystals. The dispersion of the CNC I in water was

dx.doi.org/10.1021/bm4001734 | Biomacromolecules 2013, 14, 1529−1540

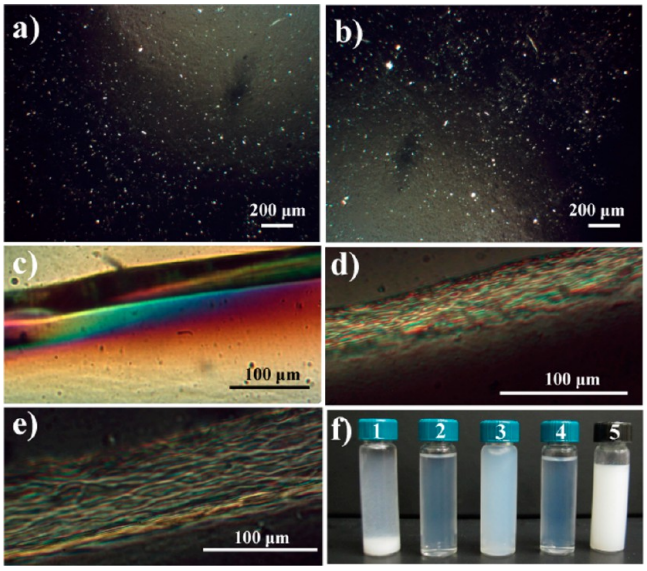

Figure 4. Aqueous suspensions of 1.0 wt % CNC I (a, c) and 1.0 wt % CNF I (b, d, and e) viewed through crossed polarizers showing the macroscopic birefringence, and the dispersion states (c) of non-homogenized cellulose suspension (1), CNC I (2), CNF I (3), CNC II (4), and CNF II (5) suspensions at the 1.0 wt % concentration (all dispersions were prepared by a 2 h stirring after preparation, and the photograph was taken after a rest of seven days).

promoted by the charged surface sulfate esters, which were generated by the reaction between hydroxyl groups of cellulose and sulfuric acid, and was further improved by the high turbulence and shear forces during HPH treatment (determined by the following optical transmittance measurement). Figure 3a revealed that homogenized CNC I were well-isolated and exhibited rod-like structure (wider at the middle than at the ends), which was a typical observation of dispersed cellulose nanocrystals.[32] The average length and width of homogenized CNC I were 149 ± 40 and 9 ± 2 nm, respectively (Table 1). These values were consistent with those of previous literatures.[4,30]

After being subjected to the combined treatment of 48 wt % H_2SO_4 and homogenization, BMP was acid-hydrolyzed into larger−sized CNF I instead of CNC I (Figure 3b). CNF I dispersed homogeneously in water and formed a stable purple colloidal suspension without visible aggregation (inset in Figures 3b and 4f). Due to stress on drying down on the substrate or induced compression or tension stress on removal from the cell wall,[33] CNF I became deformed and kink without buckling. The individual nature of CNF I can be clearly observed in Figure 3b, and CNF I oriented longitudinally in bundles. The average length and width of CNF I obtained were estimated to be 732 ± 208 and 21 ± 7 nm, respectively. Typical CNFs had a diameter in the 10−40 nm range and lengths exceeding several micrometers.[34,35] Compared with the size of reported CNFs produced from wood, the width of obtained CNF I was similar and the lengths were, however, smaller. Thus, these materials were relatively short CNFs.

The acid-hydrolysis conditions are known to affect the properties of produced cellulose particles. Longer hydrolysis time and/or increased acid-to-pulp weight ratio resulted in a smaller fiber dimension, while higher hydrolysis temperature induced some side reactions such as dehydration or carbonization, leading to dark yellow or black products.[4,36] In the present study, CNF I was ∼5 times longer in length and ∼2.5 times thicker in width compared with CNC I (Table 1). It was thus illustrated that the particle size was successfully controlled by varying the acid concentration with other conditions being optimized. During the hydrolysis in an acidic environment, the cellulose molecular chains that existed in the amorphous portions were randomly oriented in a spaghetti-like arrangement leading to a more accessible noncrystalline domain. Consequently, the acid diffused preferentially into the amorphous regions, hydrolyzed the accessible glycosidic bonds and transversely releasing individual crystallites.[36]

Because of the surface esterification of hydroxyl groups of cellulose with sulfate groups, the surfaces of CNC I and CNF I carried a mutually repulsive negative electrostatic charge (confirmed by FTIR, XPS, and ζ measurements) and thus formed stable suspensions or hydrogel in water. It was reported that the rigid rod-like cellulose I nanoparticles had a strong tendency to align along a vector director in water, creating a birefringent phenomenon that can be observed under POM.[37] The 1.0 wt % dispersions of CNC I and CNF I both showed typical birefringence when observed between crossed polarizers, thus suggesting a liquid crystalline behavior (Figure 4a−e). The birefringent nature of H_2SO_4-prepared cellulose nanoparticles depends on the suspension concentration. Interestingly, CNC I and CNF I tended to self-organize into liquid crystalline alignment at a higher concentration, leading to a stronger birefringence. After 12 h of standing, the edge of suspension sample was concentrated due to the slow evaporation of water, creating an iridescent pattern and the macroscopic birefringence (Figure 4c−e).

After BWP was subjected to mercerization treatment (20 wt % NaOH) before acid-hydrolysis (64 wt % H_2SO_4), the crystal structure of cellulose molecules was transformed from I to II (confirmed by the XRD and FTIR data above), and the resulting CNC II material is shown in Figure 3c. The morphology and dispersion state of CNC II were similar to those of CNC I (inset in Figures 3c and 4f), but their dimension was much smaller. As shown in Table 1, the average width and length of CNC II were 55 and 31% of those of CNC I, respectively. It was recently reported that the CNC II prepared by treatment of microcrystalline cellulose with sulfuric acid with controlled hydrolysis process, also tended to be shorter and thinner than the CNC I, and their size distributions were less polydispersed.[38] Presumably, the interpretation of size difference could be inferred from the mechanism of mercerization and acid-hydrolysis. The acid hydrolysis of cellulose is a heterogeneous process. During the mercerization process, the cellulose fibers were converted into a swollen state that involved formation of one or more soda−cellulose complexes in aqueous sodium hydroxide, providing larger space and more opportunities for hydronium ions to penetrate the swollen cellulose chains to break down the glycosidic bonds in amorphous regions.[24,36] In addition, after the BWP was treated with 20 wt % NaOH and then with 48% H_2SO_4, CNF II was isolated (Figure 3d). The morphology and dimension of CNF II obtained were similar to those of CNF I (Table 1). CNF II colloidal suspension was homogeneous and stable, but the color was white and turbid compared with CNF I at the same concentration (inset in Figures 3d and 4f). It was shown that the parallel-to-antiparallel reorganization of cellulose chains could also be initiated in the amorphous regions of alkali-swollen nanofibers. The molecules from adjacent cellulose I nanofibers with opposite chain polarity could then rearrange

dx.doi.org/10.1021/bm4001734 | *Biomacromolecules* 2013, 14, 1529−1540

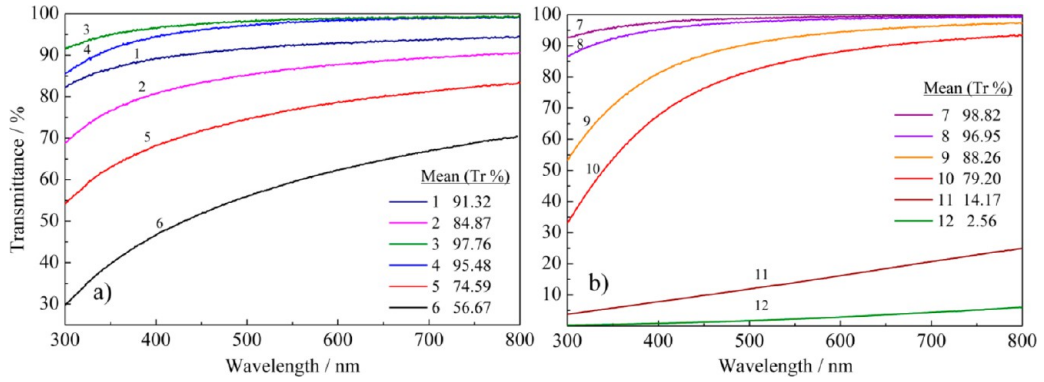

Figure 5. UV−vis transmittance spectra of water dispersions of (a) 1, 0.05 wt % N-CNC I; 2, 0.1 wt % N-CNC I; 3, 0.05 wt % CNC I; 4, 0.1 wt % CNC I; 5, 0.05 wt % CNF I; and 6, 0.1 wt % CNF I; and (b) CNC II (7, 0.05 wt %; 8, 0.1 wt %; 9, 0.5 wt %; and 10, 1.0 wt %), and CNF II (11, 0.05 wt %; and 12, 0.1 wt %).

and crystallize into antiparallel cellulose II upon being washed in water.[15]

The aspect ratio is one of the most important parameters in determining reinforcing capability of CNCs and CNFs.[19] As shown in Table 1, the corresponding aspect ratios of CNC I, CNF I, CNC II, and CNF II were 16.6, 36.6, 9.4, and 38.0, respectively. Therefore, a greater reinforcing efficiency and further applications related can be expected from these nanoparticles, especially CNF I and II.[14]

UV Optical Transmittance of Cellulose Dispersions. Figure 5a shows UV−vis light transmittance spectrum of water dispersions of nonhomogenized CNC I (N-CNC I), homogenized CNC I, and CNF I at the concentrations of 0.05 and 0.1 wt % at a visible wavelength range of 300 to 800 nm. The visible light transmittance (Tr., %) of cellulose suspension largely depends on particle size and the dispersion of particles in the aqueous suspension. At the same concentration level, the light transmittances of nonhomogenized CNC I suspensions were lower than those of homogenized CNC I suspensions in the whole measurement range of wavelength. The mean Tr. of 0.05 and 0.1 wt % CNC I suspensions were 91.32 and 84.87%, respectively. After HPH process, the mean Tr. of 0.05 and 0.1 wt % CNC I suspensions increased to 97.76 and 95.48%, respectively. Without HPH process, acid-hydrolyzed CNC I formed into larger assembled aggregates in water, leading to an undesirable dispersion of CNC I and the consequent phase separation in water (Figure 4f). When CNC I aqueous suspension was exposed under visible spectrum of sunlight, the incident light was not only absorbed within the larger CNC I aggregates, but was reflected or scattered at interfaces of separated phases, resulting in little light being transmitted through the CNC I suspension.[39] Therefore, HPH process promoted the dispersion of CNC I in water. However, the morphology of each CNC I was mostly unchanged after homogenization, suggesting that the fifth pass HPH process only dispersed CNC I but did not reduce their dimension (determined by the TEM results above). At each concentration level, CNF I suspension showed a much lower Tr. than that of CNC I suspension at 300 to 800 nm wavelength range. Compared with the CNC I suspensions, the mean Trs. of 0.1 and 0.05% CNF I suspensions decreased by 38.81 and 23.17%, respectively. This reduction in light transmission suggested that the transmittances of cellulose suspensions decreased with the increase of the size of cellulose particles. The average length of CNF I (732 nm) was almost five times longer than that of CNC I (149 nm; Table 1). When the cellulose suspension is subjected to visible light, the reflection and refraction on the surface of cellulose particle may theoretically occur if the particle size is larger than 400 nm, resulting in a loss of light transmittance.[40] This phenomenon was also demonstrated by the photographs of cellulose suspensions (insets in Figure 3). At the same concentration, the color of CNC I was much lighter than that of CNF I.

Figure 5b shows the luminous transmittance spectra of CNC II and CNF II aqueous suspensions with the concentrations from 0.05 to 1.0 wt %. The transmittance of CNC II and CNF II suspension increased with the decrease of the cellulose concentration across the whole wavelength range used. With substantially increased cellulose concentration, the probability of reflection/refraction of visible light between particles per unit volume increased, and less light was transmitted through the suspension. Consequently, the mean Tr. of CNC II suspension decreased from 98.82 to 79.20% when the cellulose concentration increased from 0.05 to 1.0 wt %. Similar results were also observed for CNC I and CNF I suspensions (Figure 5a). At each concentration level, CNF II suspension showed much lower Tr. than that of CNC II suspension at 300 to 800 nm wavelength range. Compared with the CNC II suspensions, the mean Tr. of 0.1 and 0.05 wt % CNF II suspensions decreased by 94.39 and 84.65%, respectively. This result indicated that the particle size had a stronger effect on the Tr. of cellulose II than that of cellulose I. In addition, for CNC II and CNC I, when the wavelength of incidence light ranging from 600 to 800 nm, 0.05 and 0.1% suspensions basically presented the same Tr. at each wavelength, which differed from the light transmittances at wavelength 300−600 nm. This trend indicated that, for the CNC aqueous suspension with a concentration lower than 0.1%, the concentration variation had little effect on the Tr. at wavelength 600−800 nm. Furthermore, the differences of Tr. between two crystal structures were also observed. At each concentration level, the Tr. of CNC II was slightly higher than that of CNC I over the whole range of wavelength. A possible reason was that the average length of CNC II (46 nm) was almost three times smaller than that of CNC I (149 nm; Table 1).

Surface Charges and Electrostatic Repulsion Determined by Zeta Potential and XPS Measurements. The zeta potential (ζ) has been used to study the surface charges of cellulose materials.[41] To investigate the effect of the surface charges on the lyophilization-induced self-assembling behavior

dx.doi.org/10.1021/bm4001734 | Biomacromolecules 2013, 14, 1529−1540

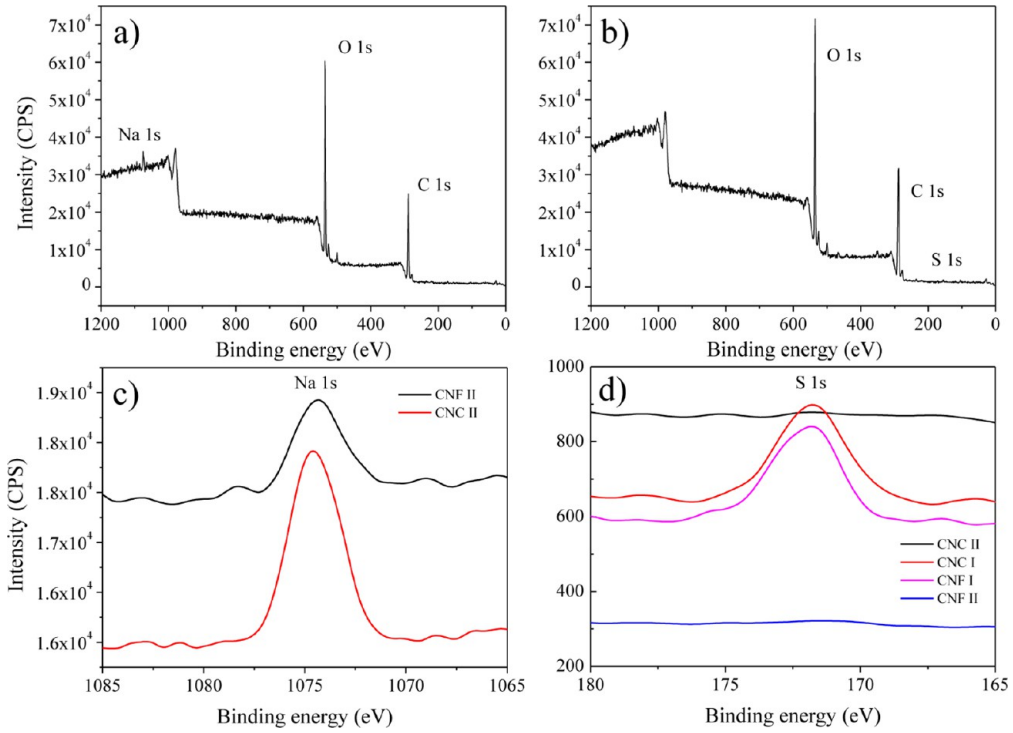

Figure 6. Typical XPS survey spectrum of CNC II (a) and CNC I (b), and comparisons of Na 1s (c) and S 2p (d) peaks for various materials.

of the obtained cellulose samples, the ζ values of CNC I, CNC II, CNF I, and CNF II in aqueous suspensions (0.05 wt %) were measured (Table 1). Based on the optical transmittance results at the same concentration, the mean Tr. of the CNF II suspension was much lower than the other samples (Figure 5), indicating that the CNF II material was not as stable as the other three samples in aqueous suspensions. The instability of CNF II in the suspension at the 0.05 wt % level made it difficult to determine its zeta potential value. Measurements on CNC I, CNC II, and CNF I showed that they carried negative electrical charges because of the presence of sulfate ester (-O-SO_3-) groups on their surfaces (also as determined from FTIR and XPS measurements). The ζ values of CNC I, CNC II, and CNF I were -57.07 ± 1.06, -0.63 ± 0.08, and -32.61 ± 1.12 mV, respectively, which were within the typical ζ range of cellulose particles as previously reported.[10,42−44] The ζ (absolute value) of CNC I was higher than that of the CNF I, indicating that CNC I carried more -O-SO_3- groups on their surfaces. No effective methods could remove the sulfate group from the sulfuric acid-hydrolyzed material completely and the esterification levels of cellulose particles highly depend on hydrolysis time and acid concentrations.[36,45] Hence, the possible reason was that higher H_2SO_4 concentration introduced more sulfate groups on the CNC I surfaces during the acid-hydrolysis process. It was also found that the ζ (absolute value) of CNC II was much lower than that of CNC I or CNF I. Therefore, the sulfur content of CNC II was much lower than that of CNC I or CNF I, which was consistent with the FTIR and XPS analysis data. Some Na^+ ions absorbed by the CNC II and CNF II during the NaOH pretreatment still remained on the fiber surfaces even after fiber washing as shown by the following XPS results (Figure 6c). It was reported previously that the absolute value of ζ and the electrostatic repulsion of cellulose nanoparticles were reduced due to the electrostatic screening effect of cation counterion Na^+.[46] Based on the double layer theories proposed by Helmholtz in 1879, the counterions in solution can shield the surface charges of particles, resulting in the screening effect of cation counterion Na^+ in acid-hydrolyzed cellulose aqueous suspension.[42] Therefore, the lower absolute value of ζ for CNC II was expected and was due to the adsorption of residue Na^+ counterions on negatively charged CNC II surfaces. It is well-known that negatively charged particles are repelled from each other, leading to the electrostatic repulsion among them. The negatively charged cellulose particles thus had mutual repulsion with each other to form an electrostatically stabilized dispersion in an aqueous suspension. Consequently, the CNC I with the higher absolute value of ζ and more sulfate charges was expected to have a stronger mutual repulsion, while the CNC II with the lower absolute value of ζ should possess a relatively weaker electrostatic repulsion with each other.

Typical XPS survey spectra of CNC II and CNC I are shown in Figures 6a and b, respectively. The peaks centered at the 535.0 and 289.0 eV positions were attributed to O 1s and C 1s, respectively. CNC II and CNF II had the peaks at 1074.5 eV corresponding to Na 1s (Figure 6c), indicating the presence of residue Na^+ ions on the surfaces of CNC II and CNF II caused by the NaOH pretreatment. The peaks at 171.0 eV were ascribed to S 2p (Figure 6d). To characterize the relative atomic percentage of S 2p for each sample, the atomic ratios of sulfur to oxygen (S/O) were calculated from corresponding peak area based on the high-resolution spectrum of S 2p. The S/O of CNC I and CNF I were 1.112 and 1.051%, respectively. The sulfur charging degrees of CNC II and CNF II were less than 0.1%. Therefore, CNC I carried more sulfate groups than CNF I, while no detectable sulfur element at the surfaces of CNC II and CNF II, confirming the results of FTIR and ζ measurements. Compared with the theoretical peak positions of S 2p (165.20 eV), O 1s (531.0 eV), C 1s (284.5 eV), and Na 1s (1071.8 eV), the measured binding energy were slightly shifted

dx.doi.org/10.1021/bm4001734 | Biomacromolecules 2013, 14, 1529−1540

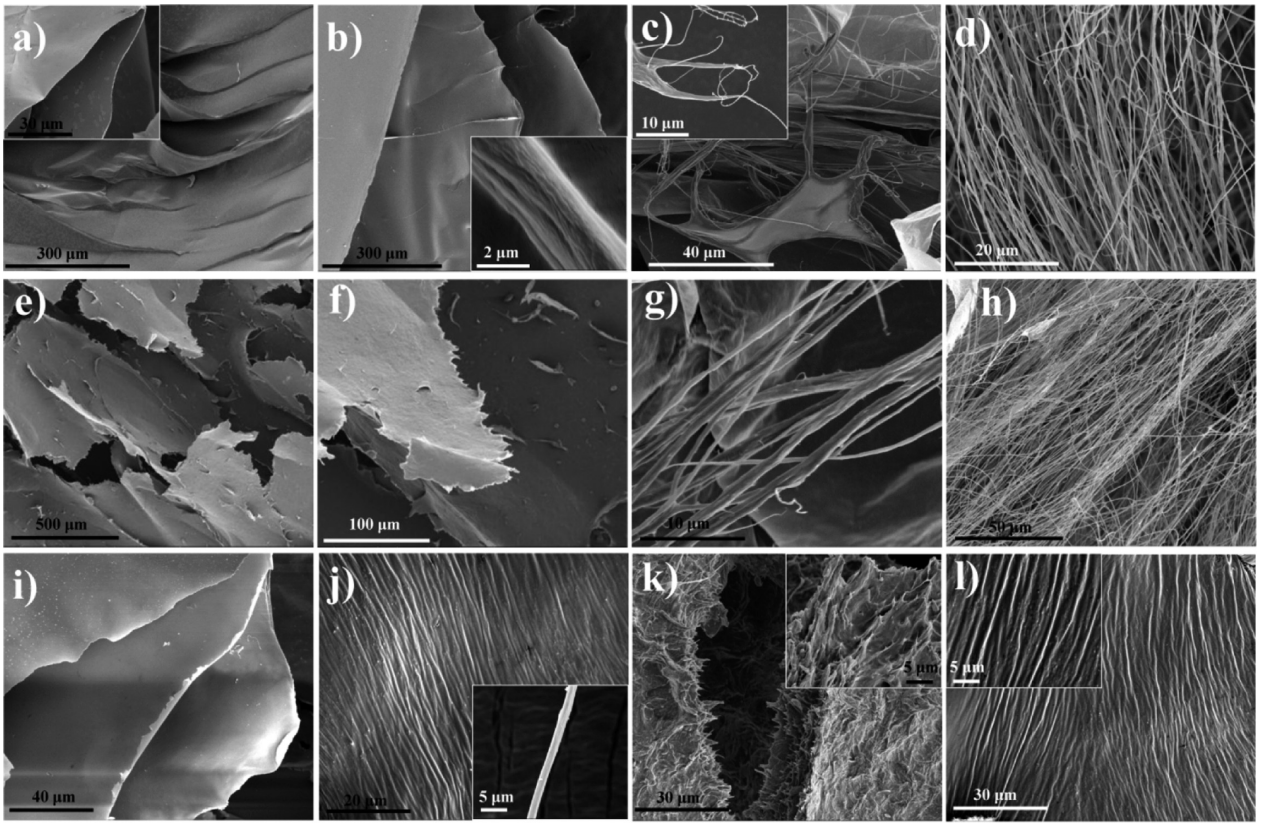

Figure 7. FE-SEM photomicrographs of freeze-dried CNC I at the concentration of 1.0 wt % (a), 0.5 wt % (b), 0.1 wt % (c), and 0.05 wt % (d), and freeze-dried CNF I at 1.0 wt % (e), 0.5 wt % (f), 0.1 wt % (g) and 0.05 wt % (h), and freeze-dried CNC II at 1.0 wt % (i), and 0.05 wt % (j), and freeze-dried CNF II at 1.0 wt % (k), and 0.05 wt % (l).

to higher values. In the present XPS measurements, cellulose samples are subjected to charging effects because of their insulating nature, resulting in the shifting of spectrum on the energy scale.

Morphology and Microstructure of Self-Assembled CNC and CNF During Freeze-Drying. It is well-known that the particle size and concentration in suspension are crucial factors for controlling morphology of freeze-dried foam.[1,8] The freeze-dried CNC I, CNC II, CNF I, and CNF II products were white and fluffy, presenting a foam structure. However, some distinctive differences of morphology and microstructure among these samples were observed by FE-SEM at the micrometer scale (Figure 7a–l).

For the freeze-dried CNC I at the concentrations of 0.5 and 1.0 wt %, the lamellar structured foam composed of aligned thin membrane layers with width between 0.5 and 3 μm was fabricated (Figure 7a,b). Each layer was created in parallel to each other and presented a smooth surface and homogeneous character throughout the entire layer. It can be clearly seen that these layers actually consisted of oriented microsized cellulose fibers with an average diameter of 1–3 μm (inset in Figure 7b). This result indicated that nanosized CNC I (149 ± 40 nm in length and 9 ± 2 nm in width) were first longitudinally self-assembled into the larger-sized cellulose fibers that were further self-organized in parallel to form a film-like structure during freeze-drying. The significant coalescence of cellulose subunits caused by freeze-drying process was reported previously.[47,48] Compared with a similar observation reported by Sehaqui et al.,[35] the layers we obtained had a higher compactness and no visible porosity was seen. Freeze-drying 0.5 and 1.0 wt % CNF I aqueous suspensions resulted in similar layered structure (Figure 7e,f), indicating that CNF I also showed the self-organizing phenomenon. However, the fracture surface of CNF I was not as smooth as that of CNC I and visible dendrites stood out from the fractured surface, presumably due to the lager dimensions of CNF I. This result revealed that the CNC dimensions had an important effect on the lyophilization-induced self-assembly behaviors. At high concentration levels (0.5–1.0 wt %), larger size CNF I could hardly form the smooth surface and presented homogeneous character throughout the entire layer.

After the concentration was diluted to 0.05 wt %, the CNC I and CNF I aqueous suspensions both self-assembled into oriented ultrafine fibers with diameters of 0.57 ± 0.17 and 1.02 ± 0.27 μm instead of sheet-like structure by sublimating ice molecules (Figure 7d,h). The mean diameter of ultrafine fibers formed by CNF I was twice as much as that of CNC I, indicating that the diameter of self-assembled ultrafine fibers increased with the dimension of cellulose particles at the 0.05 wt % concentration level. In addition, the zeta potential and XPS results all revealed that more sulfate groups were introduced onto the surfaces of CNC I compared with CNF I, resulting in a stronger electrostatic repulsion between CNC I. It is thus inferred that the weaker mutual repulsion of CNF I can promote their self-organization into ultrafine fibers. Therefore, at the 0.05 wt % concentration level, more surface charges of cellulose nanoparticles led to the smaller diameters of self-assembled ultrafine fibers. A similar effect of surface charges on the lyophilization-induced self-assembling behavior was further observed between CNC II and CNC I at the 0.05

dx.doi.org/10.1021/bm4001734 | *Biomacromolecules* 2013, 14, 1529–1540

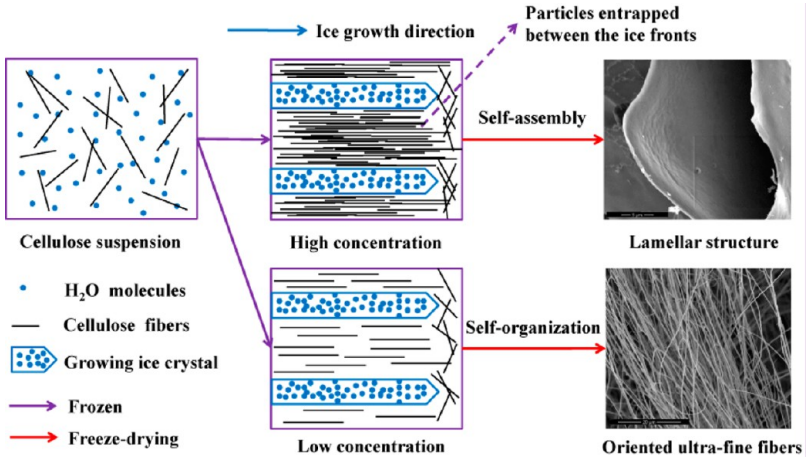

Figure 8. Schematic of possible formation mechanism of the lamellar geometry and the alignment of ultrafine fibers during the freeze-drying process.

wt % concentration level. It was also found that the widths of self-assembled ultrafine fibers were much narrower than those of fiber clusters found in original BWP (Table 1). The similar intriguing self-assembling behavior of dilute CNC suspensions prepared from rice straw was reported by Lu and Hsieh.[9] They obtained the ultrafine cellulose fibers from acid-hydrolyzed rice straw with a mean width of ~0.386 μm under a different freeze-drying condition. However, the long cellulose fibers they obtained were randomly arranged into a network structure instead of an oriented arrangement in the present research. One reason is the difference of cellulose source, and the other reason is the variation of freezing conditions. They quickly froze the samples by adding liquid nitrogen, whereas the dilute cellulose suspension was frozen in a freezer at −75 °C for 2 h in this study, which allowed the oriented self-organizing behavior of ultrafine fibers to occur during this time. In this way, the cellulose particles had enough time to adjust and rearrange their position during the freezing process. The self-assembly mechanism of cellulose during freeze-drying was detailed below.

The hydrogen bonding arrangement plays an important role in the self-assembling properties of cellulose suspension. Therefore, the difference of hydrogen bonding systems between cellulose I and II is thought to affect the self-organizing behavior of cellulose particles in aqueous suspension during freeze-drying process. However, lyophilization-induced self-assembling behavior of cellulose II has not been thoroughly reported in the literature so far. To investigate the effect of cellulose crystal structure on the self-assembling behavior of cellulose nanoparticles, CNC II and CNF II aqueous suspensions at the concentration of 0.05 and 1.0 wt % were freeze-dried. For the freeze-dried CNC II at the concentration of 0.05 wt %, many microsized cellulose fibers with an average diameter of ~1.5 μm were found (Figure 7j). When the concentration was increased to 1.0 wt %, a lamellar structured foam composed of thin membrane layers was created (Figure 7i). This layered-structure morphology was identical with that of freeze-dried CNC I at the same concentration (Insert in Figure 7a), indicating that cellulose crystal structure had insignificant effect on the self-assembling properties of 1.0 wt % CNC suspensions. For the freeze-dried CNF II at the concentration of 0.05 wt %, CNF II aqueous suspensions self-assembled into highly oriented ultrafine fibers with diameters of ~1 μm (Figure 7l). This phenomenon was also found in freeze-dried 0.05 wt % CNF I suspension (Figure 7h). At the concentration of 1.0 wt %, many aligned macro-sized cellulose fibers stood out from the fractured surface of freeze-dried CNF II (Figure 7k). In fact, these layers were composed of oriented macrosized cellulose fibers when it was observed along the perpendicular to aligned direction (inset in Figure 7k). However, the surface of CNF II was not as homogeneous as that of CNF I, presumably because of different cellulose crystal structure.

Mechanism of Lyophilization-Induced Self-Assembling Behavior of Cellulose Particles. A possible mechanism could be inferred from the basic physics of ice crystal growth, the interaction between cellulose particles, and the chiral nematic anisotropic nature of liquid crystalline polymer. Figure 8 shows a scheme presenting the formation mechanism of the lamellar geometry and the alignment of ultrafine fibers in the freeze-drying process. Before steady-state freezing process, CNCs and CNFs in water formed stable and homogeneous aqueous suspensions because of the interparticle electrostatic repulsion provided by the negatively charged sulfate groups on the surfaces of cellulose particles. When a cellulose suspension with suitable granulometry was frozen under steady-state conditions, ice crystals gradually grew in the same direction as the temperature gradient and created a lamellar microstructure oriented in a direction parallel to the movement of the freezing front.[1,8] Simultaneously, the cellulose particles were expelled from the growing ice crystals and squeezed into the space between ice crystals or dendrites. Consequently, the concentration of cellulose particles increased in the space among growing ice crystals during the freezing of water. When the critical concentration of sulfated cellulose necessary for the formation of ordered nematic phases was reached (typically 1.0 to 10 wt %), the rod-like cellulose particles spontaneously formed ordered structure in the space between growing ice crystals.[3] Once the freezing process was completed, the original homogeneous suspension system was destroyed and transformed into an ice-template structure by the lyophilization-induced physical interaction. During the freeze-drying process, ice molecules were gradually sublimated from the lamellar ice-template system. As a result, the suspended cellulose particles were concentrated and trapped in the space between these ice crystals, generating a replica of the original ice-template.[1] These concentrated cellulose particles compactly rearranged and well self-assembled along the longitudinal direction into larger-sized cellulose microfibers via strong hydrogen bonds and van der Waals forces.[1,2] It was reported

dx.doi.org/10.1021/bm4001734 | Biomacromolecules 2013, 14, 1529−1540

that the cellulose nanocrystals were well aligned along the axis of each self-assembled fiber.[9] In addition, the ends of these ultrafine fibers were not prevalent in the SEM observations (Figure 7d,h,j,l), indicating the lengths of these self-assembled cellulose fibers probably reached millimeter-scale. For highly concentrated suspensions (0.5−1.0 wt %), the gap between the self-assembled microfibers was small enough for the formation of hydrogen bonding and tight bonds with neighboring microfibers, and these adjacent microfibers aligned along the freezing direction to form a dense layered structure due to the linking with adsorbed/bound water and the momentum exerted by growing ice crystals.[1,49] By contrast, the space between self-assembled microfibers became larger when the concentration of suspensions was diluted to the 0.05 wt % level, resulting in the weakening of hydrogen bonding and interfacial attraction between microfibers. In addition, rod-like cellulose particles tended to spontaneously form parallel configuration in diluted aqueous medium since the effective excluded volume is zero.[50] Therefore, the 0.05 wt % CNC and CNF aqueous suspensions both self-assembled into oriented ultrafine fibers instead of sheet-like structure during lyophilization (Figure 7d,h,j,l). At the semidilute concentration (0.1 wt %), self-assembled layers and oriented ultrafine fibers coexisted in the foam (Figure 7c,g), presenting an intermediate stage of the structure transition from membrane layers to oriented ultrafine fibers. The inset in Figure 7c showed that the membrane layers obtained were composed of self-assembled ultrafine cellulose fibers.

In addition, at the concentration of 0.05 wt %, the average diameter of ultrafine fibers assembled from CNC II was larger than that from CNC I. Because the mean width of CNC I was almost twice as long as CNC II, the estimated quantity of CNC II within the cross section of each ultrafine fiber was much more than that of CNC I. This distinction of self-assembling behavior might be induced by the different intra- and interhydrogen bonding patterns within cellulose I and II molecular chains. Cellulose I has two intramolecular hydrogen bonds at (O)6−(OH)2 and (O)5−(OH)3, and an interchain hydrogen bond between (O)6−(O)3. When the cellulose fibers are swollen in a NaOH solution, the hydrated hydroxide ions penetrate the internal crystals, and cause the chain rearrangements from parallel cellulose I to antiparallel cellulose II with a changed inter/intrahydrogen bonding networks. Cellulose II possesses an intrachain hydrogen bonding at (O)5−(OH)3 and two intermolecular hydrogen bond at (O)2−(OH)6 and (O)3−(OH)6. Besides, an intersheet interaction between (O)2−(OH)2 that is absent in cellulose I also exists in cellulose II hydrogen bonding system.[51] Furthermore, the hydrogen bonds in cellulose II (average bond length of 0.272 nm) is shorter and stronger those in cellulose I (average bond length of 0.280 nm).[52] Besides, IR index values showed that CNC II had more hydroxyl groups on the crystal surface (Determined by FTIR results). These factors probably promoted the congregating and self-assembly of CNC II. However, the effect of crystal structure on the self-assembling behavior reduced with the increasing concentration. At the concentration of 1 wt %, the layered-structure morphology self-assembled from cellulose II was almost identical with that of CNC I. As discussed before, in addition to the particle size and crystal structure, less surface charges can promote the lyophilization-induced self-assembling behavior of cellulose nanoparticles. Based on the FTIR, zeta potential, and XPS results, less negatively charged CNC II possess a relatively weaker mutual electrostatic repulsion than CNC I. As a consequence, CNC II was easier to self-assemble into wider ultrafine fibers than CNC I.

CONCLUSIONS

CNCs and short CNFs with cellulose I and II crystalline allomorphs were extracted from BWP. The particle size, crystal structure, and dispersion state were successfully controlled by using different acid concentration, alkaline pretreatment, and high-pressure homogenization. Cellulose concentration, particle size, surface charge, and crystal structure significantly influenced the lyophilization-induced self-assembling behavior of the cellulose suspensions. During freeze-drying, at higher suspension concentrations, the gap between the self-assembled microfibers was small enough for the formation of hydrogen bonding and tight bonds with neighboring microfibers, and these adjacent microfibers aligned along the freezing direction to form lamellar structured foam composed of aligned thin membrane layers. At diluted concentrations, due to the weakening of hydrogen bonding and interfacial attraction among the fibers, cellulose particles self-assembled into highly oriented ultrafine fibers with different diameters, instead of the sheet-like structure. The congregating and self-assembly of cellulose particles were promoted by larger particle size, weaker mutual electrostatic repulsion, and more hydroxyl groups on their surface, resulting in a larger size of self-assembled fibers.

By freezing aqueous suspensions containing cellulose particles under suitable conditions, we demonstrated the possibility of building homogeneous scaffolds with aligned membrane layers or forming oriented ultrafine fibers, opening their use as a template for fine-structure composites. Because of the tight association of the cellulose particles through the abundant intercrystal hydrogen bonds, self-organized cellulose products induced by lyophilization presented extraordinary structural stability and integrity in aqueous media under mechanical stirring.[9] For this reason, the morphology and structure of freeze-dried foam can be controlled by adjusting cellulose concentration, crystal structure, surface charges, and particle size to obtain a tailored template, showing great promises for many potential applications, such as tissue engineering scaffolds or new biomaterials for orthopedic applications.[2,8,52]

AUTHOR INFORMATION

Corresponding Author

*E-mail: qwu@agcenter.lsu.edu. Phone: 225-578-8369. Fax: 225-578-4251.

Notes

The authors declare no competing financial interest.

ACKNOWLEDGMENTS

The authors are thankful for the financial support from Louisiana Board of Regents [LEQSF-EPS(2013)-PFUND-318 and (LEQSF(2010-13)-RD-B-01] and Chinese Scholarship Council (CSC No.: 2009660015), and for the generous support from Dr. Ward Plummer, LSU Department of Physics, in XPS analysis .

REFERENCES

(1) Lee, J.; Deng, Y. L. *Soft Matter* **2011**, *7*, 11547−11547.
(2) Dash, R.; Li, Y.; Ragauskas, A. J. *Carbohydr. Polym.* **2012**, *88*, 789−792.
(3) Habibi, Y.; Lucia, L. A.; Rojas, O. J. *Chem. Rev.* **2010**, *110*, 3479−3500.

(4) Beck-Candanedo, S.; Roman, M.; Gray, D. G. *Biomacromolecules* **2005**, *6*, 1048−1054.
(5) Bondeson, D.; Mathew, A.; Oksman, K. *Cellulose* **2006**, *13*, 171−180.
(6) Peng, Y. C.; Gardner, D. J.; Han, Y. S. *Cellulose* **2012**, *19*, 91−102.
(7) Svagan, A. J.; Samir, M. A. S. A.; Berglund, L. A. *Adv. Mater.* **2008**, *20*, 1263−1269.
(8) Deville, S.; Saiz, E.; Nalla, R. K.; Tomsia, A. P. *Science* **2006**, *311*, 515−518.
(9) Lu, P.; Hsieh, Y. L. *Carbohydr. Polym.* **2012**, *87*, 564−573.
(10) Boluk, Y.; Zhao, L. Y.; Incani, V. *Langmuir* **2012**, *28*, 6114−6123.
(11) Segal, L.; Creely, J. J.; Martin, A. E.; Conrad, C. M. *Text. Res. J.* **1959**, *29*, 786−794.
(12) Elazzouzi-Hafraoui, S.; Nishiyama, Y.; Putaux, J. L.; Heux, L.; Dubreuil, F.; Rochas, C. *Biomacromolecules* **2008**, *9*, 57−65.
(13) Uetani, K.; Yano, H. *Langmuir* **2012**, *28*, 818−827.
(14) Kamphunthong, W.; Hornsby, P.; Sirisinha, K. *J. Appl. Polym. Sci.* **2012**, *125*, 1642−1651.
(15) Zuluaga, R.; Putaux, J. L.; Cruz, J.; Velez, J.; Mondragon, I.; Ganan, P. *Carbohydr. Polym.* **2009**, *76*, 51−59.
(16) Johar, N.; Ahmad, I.; Dufresne, A. *Ind. Crop Prod.* **2012**, *37*, 93−99.
(17) Moran, J. I.; Alvarez, V. A.; Cyras, V. P.; Vazquez, A. *Cellulose* **2008**, *15*, 149−159.
(18) Ouajai, S.; Shanks, R. A. *Polym. Degrad. Stab.* **2005**, *89*, 327−335.
(19) Wang, B.; Sain, M.; Oksman, K. *Appl. Compos. Mater.* **2007**, *14*, 89−103.
(20) Li, R. J.; Fei, J. M.; Cai, Y. R.; Li, Y. F.; Feng, J. Q.; Yao, J. M. *Carbohydr. Polym.* **2009**, *76*, 94−99.
(21) Sao, K. P.; Mathew, M. D.; Ray, P. K. *Text. Res. J.* **1987**, *57*, 407−414.
(22) Oh, S. Y.; Yoo, D. I.; Shin, Y.; Kim, H. C.; Kim, H. Y.; Chung, Y. S.; Park, W. H.; Youk, J. H. *Carbohydr. Res.* **2005**, *340*, 2376−2391.
(23) Gwon, J. G.; Lee, S. Y.; Doh, G. H.; Kim, J. H. *J. Appl. Polym. Sci.* **2010**, *116*, 3212−3219.
(24) Dinand, E.; Vignon, M.; Chanzy, H.; Heux, L. *Cellulose* **2002**, *9*, 7−18.
(25) Wang, M. J.; Xie, Y. L.; Zheng, Q. D.; Yao, S. J. *Ind. Eng. Chem. Res.* **2009**, *48*, 5276−5284.
(26) Yue, Y. Y.; Zhou, C. J.; French, A. D.; Xia, G.; Han, G. P.; Wang, Q. W.; Wu, Q. L. *Cellulose* **2012**, *19*, 1173−1187.
(27) Liu, Y. P.; Hu, H. *Fibers Polym.* **2008**, *9*, 735−739.
(28) Lu, P.; Hsieh, Y. L. *Carbohydr. Polym.* **2010**, *82*, 329−336.
(29) Mahadeva, S. K.; Kim, J. *J. Phys. Chem. C* **2009**, *113*, 12523−12529.
(30) Liu, H. Y.; Liu, D. G.; Yao, F.; Wu, Q. L. *Bioresour. Technol.* **2010**, *101*, 5685−5692.
(31) Han, J.; Zhou, C.; French, A. D.; Han, G.; Wu, Q. *Carbohydr. Polym.* **2013**, *94*, 773−781.
(32) Kvien, I.; Tanem, B. S.; Oksman, K. *Biomacromolecules* **2005**, *6*, 3160−3165.
(33) Manley, R. S. J. *Nature* **1964**, *204*, 1155−1157.
(34) Henriksson, M.; Berglund, L. A.; Isaksson, P.; Lindstrom, T.; Nishino, T. *Biomacromolecules* **2008**, *9*, 1579−1585.
(35) Sehaqui, H.; Salajkova, M.; Zhou, Q.; Berglund, L. A. *Soft Matter* **2010**, *6*, 1824−1832.
(36) Dong, X. M.; Revol, J. F.; Gray, D. G. *Cellulose* **1998**, *5*, 19−32.
(37) Lima, M. M. D.; Borsali, R. *Macromol. Rapid Commun.* **2004**, *25*, 771−787.
(38) Sebe, G.; Ham-Pichavant, F.; Ibarboure, E.; Koffi, A. L. C.; Tingaut, P. *Biomacromolecules* **2012**, *13*, 570−578.
(39) Yu, Z. J.; Jiang, Y. Q.; Zou, W. W.; Duan, J. J.; Xiong, X. P. *J. Polym. Sci., Part B: Polym. Phys.* **2009**, *47*, 1686−1694.
(40) Tang, C. Y.; Liu, H. Q. *Composites, Part A* **2008**, *39*, 1638−1643.
(41) Iyer, S. R. S.; Jayaram, R. *J. Soc. Dyers Colour.* **1971**, *87*, 338−342.
(42) Boluk, Y.; Lahiji, R.; Zhao, L. Y.; McDermott, M. T. *Colloids Surf., A* **2011**, *377*, 297−303.
(43) Teixeira, E. D.; Correa, A. C.; Manzoli, A.; Leite, F. L.; de Oliveira, C. R.; Mattoso, L. H. C. *Cellulose* **2010**, *17*, 595−606.
(44) Hasani, M.; Cranston, E. D.; Westman, G.; Gray, D. G. *Soft Matter* **2008**, *4*, 2238−2244.
(45) Gu, J.; Catchmark, J. M.; Kaiser, E. Q.; Archibald, D. D. *Carbohydr. Polym.* **2013**, *92*, 1809−1816.
(46) Zhong, L. X.; Fu, S. Y.; Peng, X. W.; Zhan, H. Y.; Sun, R. C. *Carbohydr. Polym.* **2012**, *90*, 644−649.
(47) Deng, M. L.; Zhou, Q.; Du, A. K.; van Kasteren, J.; Wang, Y. Z. *Mater. Lett.* **2009**, *63*, 1851−1854.
(48) Jin, H.; Nishiyama, Y.; Wada, M.; Kuga, S. *Colloids Surf., A* **2004**, *240*, 63−67.
(49) Liu, D. G.; Chen, X. Y.; Yue, Y. Y.; Chen, M. D.; Wu, Q. L. *Carbohydr. Polym.* **2011**, *84*, 316−322.
(50) Eichhorn, S. J. *Soft Matter* **2011**, *7*, 303−315.
(51) O'Sullivan, A. C. *Cellulose* **1997**, *4*, 173−207.
(52) Jiang, W.; Sun, L. F.; Hao, A. Y.; Chen, J. Y. *Text. Res. J.* **2011**, *81*, 1949−1958.
(53) Hench, L. L.; Polak, J. M. *Science* **2002**, *295*, 1014−1017.